



Analysis of conductivity and dielectric spectra of $\text{Mn}_{0.5}\text{Zn}_{0.5}\text{Fe}_2\text{O}_4$ with coupled Cole–Cole type anomalous relaxations

N.S.K. Kumar, T.S. Shahid, G. Govindaraj*

Department of Physics, School of Physical, Chemical and Applied Sciences, Pondicherry University, Puducherry 605014, India

ARTICLE INFO

Article history:

Received 24 March 2015
 Received in revised form
 1 February 2016
 Accepted 8 February 2016
 Available online 19 February 2016

Keywords:

Impedance/dielectric spectroscopy
 Hopping conduction
 Non-Debye dispersion

ABSTRACT

Most of the crystalline materials seldom show a well-defined dielectric loss peak due to domination of dc conductivity contribution, but effects of loss peaks are seen at high frequencies. Ac electrical data of nano-crystalline $\text{Mn}_{0.5}\text{Zn}_{0.5}\text{Fe}_2\text{O}_4$ synthesised by chemical co-precipitation method show such behaviour. Properly combined and formulated conduction and dielectric relaxation functions are required for such materials. Cole–Cole type relaxation function in the combined conduction and dielectric process is formulated for complex resistivity $\rho^*(\omega)$, complex permittivity $\epsilon^*(\omega)$, complex conductivity $\sigma^*(\omega)$ and complex electric modulus $M^*(\omega)$. Conduction and dielectric relaxation are linked to Jonscher's idea of 'pinned dipole' and 'free dipole' to understand the relaxation dynamics. The physical parameters of 'pinned dipole' and 'free dipole' formalism are unique for all representations like $\rho^*(\omega)$, $\epsilon^*(\omega)$, $\sigma^*(\omega)$ and $M^*(\omega)$. 'Pinned dipole' relaxation time τ_c related to conduction process and 'free dipole' relaxation time τ_d related to dielectric process show Arrhenius behaviour with the same activation energy. Correlation of dc conductivity σ_c with τ_c and τ_d indicates the coupled dynamics of 'pinned dipole' and 'free dipole'. Time-temperature scaling of conduction and dielectric relaxation reveals that the mechanism of coupled dynamics of 'pinned dipole' and 'free dipole' is temperature independent. Hopping of charge carriers with dynamics of disordered cation distribution of host matrix generates a coupled conduction and dielectric relaxation in $\text{Mn}_{0.5}\text{Zn}_{0.5}\text{Fe}_2\text{O}_4$.

© 2016 Elsevier B.V. All rights reserved.

$$\epsilon_{\text{tot}}^*(\omega) = \frac{\sigma_c(1 + (i\omega\tau_c)^{\alpha_c})}{i\epsilon_0\omega} + \frac{\epsilon_d}{1 + (i\omega\tau_d)^{\alpha_d}} + \epsilon_\infty$$

1. Introduction

Impedance spectroscopy is one of the suitable tools to investigate electrical property of the materials for a broad range of frequency. Materials such as liquids, polymers, ionic conducting solids and even disordered semiconductors are analysed with broadband dielectric spectroscope. Dielectric relaxation loss peak is observed in liquids, glass forming-liquids and polymers for broad frequency range for various temperatures [1,2]. The dc conductivity σ_{dc} contributes to the dielectric loss $\sigma_{dc}/(\epsilon_0\omega)$. The dielectric relaxation and σ_{dc} contribution are well separated since dc conductivity contributes well below the dielectric loss peaks in these materials. The dielectric relaxation process and dc conductivity are related by Debye–Stokes–Einstein (DSE) relation. The dielectric process in most of the liquids and glass forming liquids is decoupled with dc conductivity by fractional power of DSE relation [3,4]. Most of the inorganic ion conducting glasses [5,6], and poly crystalline materials [7,8], not often shows a well-defined loss peak since dc conductivity contribution dominates the dielectric

loss peak, but the dielectric relaxation effects are seen at high frequencies in some materials [9,10]. Semiconducting ferrites [11] are one among the materials having conductivity contribution with an effect of dielectric relaxation at high frequencies.

Different schools discuss similar experimental facts with their preferred way of presenting data. Dielectric constant $\epsilon^*(\omega)$ is preferred by dielectric school, and semiconducting school prefers $\sigma^*(\omega)$ to present experimental data. Representing data into electric modulus $M^*(\omega)$ and complex impedance $Z^*(\omega)$ are also popular [12]. Which is the best representation of ac data, is still controversially debated [13–16]. All these representations are related to each other and have the same information of electrical property. Hence proper model of relaxation should necessarily follow all these representations.

In mixed ferrite, cation distribution of tetrahedral (A-site) and octahedral (B-site) plays a dominant role in structural, electrical and magnetic properties of nano-phase materials [17–23]. It is evident from the previous studies that the cation distribution can lead to peculiar electrical behaviour such as semiconductor to metal transition and polaron conduction [17–20]. Ac conductivity of disordered solids shows approximate power law behaviour and exponent varies weakly with frequency [24]. It is reported that ac conductivity of disordered ionic conducting solids may consist of

* Corresponding author.

E-mail address: ggraj_7@yahoo.com (G. Govindaraj).

contributions from the hopping charge conduction and local relaxation motion of host matrix [25,26]. Molecular level understanding of this combined relaxations is still challenging.

In the present work, nano-crystalline $\text{Mn}_{0.5}\text{Zn}_{0.5}\text{Fe}_2\text{O}_4$ (MZFO) is synthesised by chemical co-precipitation method and characterised with XRD and Raman spectra. Ac electrical measurements of MZFO were carried out by obtaining complex impedance data in the frequency range 1 Hz–3 MHz and in the temperature range 303–503 K. The ac electrical data are analysed with combined ‘pinned dipole’ and ‘free dipole’ relaxation. The salient features of the present study are:

1. MZFO shows dielectric loss peak in which dc conductivity is dominated.
2. Cole–Cole type conduction and dielectric relaxation are integrated and hence semiconducting and dielectric school thoughts are combined.
3. The electrical parameters are shown to be independent of ac data representations.
4. The relaxation of hopping charge and its host matrix of MZFO show coupled relaxation dynamics.

2. Experiment

Wet chemical co-precipitation method was used to synthesise $\text{Mn}_{0.5}\text{Zn}_{0.5}\text{Fe}_2\text{O}_4$ nano-particles. A.R. grade $\text{MnCl}_2 \cdot 4\text{H}_2\text{O}$, ZnCl_2 and FeCl_3 were used as precursors and NaOH as a precipitation agent. 1600 ml solution of 0.5 M NaOH was prepared using doubly distilled water and kept for boiling. 100 ml solution of MnCl_2 , ZnCl_2 and FeCl_3 were mixed together under magnetic stirring at 700 rpm to form a homogeneous solution and slowly heated to 80 °C. This solution was poured quickly to the boiling solution of NaOH and pH was adjusted to 11. The mixture was stirred at 100 °C for 1 h to form ferrite particles. Thus obtained sample was centrifuged and washed several times until the formation of pure sample, free from sodium or chloride ions. The prepared sample was dried for 12 h using heating mantle.

Powder X-ray diffraction of sample was taken at room temperature with X’pert PANalytical X-ray diffractometer with $\text{CuK}\alpha$ radiation of wavelength $\lambda = 1.5418 \text{ \AA}$. The XRD results confirmed the formation of cubic inverse spinel structured MZFO. Lattice parameters $a = b = c = 8.397 \text{ \AA}$ are obtained with *celref* software. The XRD pattern of the sample is shown in Fig. 1. The average crystalline size of MZFO, obtained through Scherrer’s formula, is 11 nm which can be considered as the lower bound on the particle size since Scherrer’s formalism neglects strain and local disorder contributions to broadening.

Raman spectroscopic measurement has been carried out at room temperature with 530 nm radiation. Raman shift of the range of 200–800 cm^{-1} with individual Lorentzian components is shown in Fig. 2. Ferrite with cubic inverse spinel of type AB_2O_4

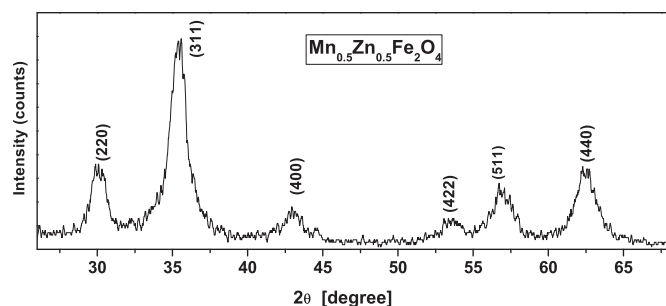


Fig. 1. X-ray diffraction pattern of MZFO.

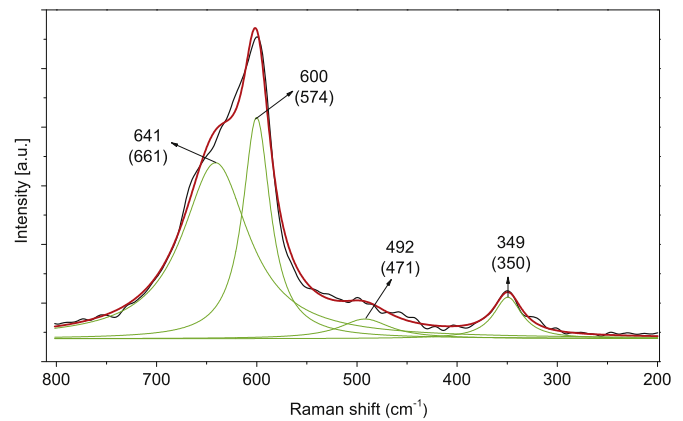


Fig. 2. Raman shift of MZFO as a function of wave number. Individual Raman mode of MZFO is indicated in comparison of Ref. [21] is shown in brackets.

belonging to $\text{Fd}3\text{m}$ space groups has five Raman active modes. The present sample shows four prominent Raman active modes as reported earlier [21], but with slightly different band positions. Strain and loss of symmetry affect the band position and broadening of Raman mode. In nano-crystalline mixed ferrite, strain and loss of symmetry may originate from the presence of vacancies, lattice defects and disordered cation distribution.

The sample pellet of diameter 12.84 mm and thickness 1 mm is placed in the gold plated electrodes. Complex impedance data were taken with Novocontrol broadband dielectric spectrometer for the frequency range of 1 Hz–3 MHz for various temperatures. The sample is heated to a temperature 503 K and obtained electrical data by cooling down to 303 K with 20 K steps.

3. Results and discussion

3.1. Combined conduction and dielectric relaxation formalism

The impedance/dielectric spectroscopy measures the magnitude of current and phase difference with respect to the applied electric field for various frequencies. Hence obtained $I^*(\omega) = V^*(\omega)/Z^*(\omega)$ can be transformed to complex impedance $Z^*(\omega)$ or complex capacitance $C^*(\omega) = 1/i\omega Z^*(\omega)$. This is used to generate different representations [27,28] such as $\epsilon^*(\omega)$, $\sigma^*(\omega)$ and $M^*(\omega)$. Materials which possess ‘pinned dipole’ and ‘free dipole’ relaxation can be modelled with an equivalent circuit as shown in Fig. 3.

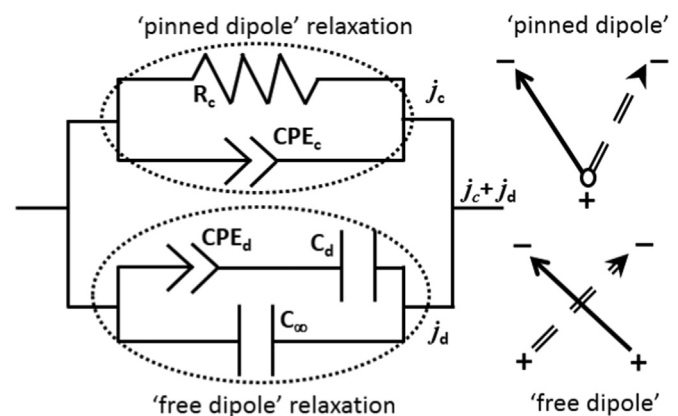


Fig. 3. Equivalent circuit of material possessing Cole–Cole type anomalous conduction and dielectric relaxation. Thematic representation of ‘pinned dipole’ and ‘free dipole’ corresponding to the conduction and dielectric relaxation respectively is shown.

Table 1
Physical parameters of conduction and dielectric relaxation of MZFO At various temperatures.

T (K)	Conduction relaxation			Dielectric relaxation			
	σ_c (S/cm)	τ_c (s)	α_c	ϵ_d	τ_d (s)	α_d	ϵ_∞
303	$(1.603 \pm 0.008) \times 10^{-10}$	$(3.1 \pm 0.3) \times 10^{-3}$	0.818 ± 0.006	20.6 ± 0.9	$(1.7 \pm 0.3) \times 10^{-3}$	0.617 ± 0.012	7.70 ± 0.02
323	$(5.320 \pm 0.021) \times 10^{-10}$	$(9.4 \pm 0.9) \times 10^{-4}$	0.829 ± 0.005	20.4 ± 0.8	$(4.8 \pm 0.9) \times 10^{-4}$	0.628 ± 0.012	7.61 ± 0.02
343	$(1.583 \pm 0.006) \times 10^{-9}$	$(3.2 \pm 0.4) \times 10^{-4}$	0.837 ± 0.005	20.1 ± 0.7	$(1.6 \pm 0.4) \times 10^{-4}$	0.639 ± 0.012	7.47 ± 0.02
363	$(4.291 \pm 0.012) \times 10^{-9}$	$(1.2 \pm 0.1) \times 10^{-4}$	0.856 ± 0.004	20.2 ± 0.6	$(5.6 \pm 0.9) \times 10^{-5}$	0.652 ± 0.010	7.11 ± 0.02
383	$(1.010 \pm 0.002) \times 10^{-8}$	$(5.2 \pm 0.6) \times 10^{-4}$	0.870 ± 0.004	21.7 ± 0.6	$(2.5 \pm 0.5) \times 10^{-5}$	0.644 ± 0.008	6.89 ± 0.01
403	$(2.385 \pm 0.004) \times 10^{-8}$	$(2.1 \pm 0.3) \times 10^{-5}$	0.893 ± 0.006	22.9 ± 0.6	$(1.1 \pm 0.2) \times 10^{-5}$	0.634 ± 0.008	6.6^a
423	$(5.536 \pm 0.009) \times 10^{-8}$	$(8.3 \pm 0.9) \times 10^{-6}$	0.915 ± 0.009	23.1 ± 0.8	$(4.6 \pm 0.9) \times 10^{-6}$	0.637 ± 0.010	6.4^a
443	$(1.157 \pm 0.001) \times 10^{-7}$	$(3.9 \pm 0.6) \times 10^{-6}$	0.930 ± 0.006	24.0 ± 0.5	$(2.3 \pm 0.4) \times 10^{-6}$	0.634 ± 0.006	6.1^a
463	$(2.184 \pm 0.002) \times 10^{-7}$	$(2.4 \pm 0.3) \times 10^{-6}$	0.924 ± 0.005	24.3 ± 0.4	$(1.3 \pm 0.2) \times 10^{-6}$	0.632 ± 0.005	5.8^a
483	$(4.196 \pm 0.003) \times 10^{-7}$	$(1.3 \pm 0.1) \times 10^{-6}$	0.924 ± 0.004	23.9 ± 0.4	$(6.8 \pm 0.9) \times 10^{-7}$	0.638 ± 0.005	5.6^a
503	$(7.945 \pm 0.004) \times 10^{-7}$	$(7.3 \pm 0.6) \times 10^{-7}$	0.929 ± 0.003	23.3 ± 0.3	$(3.6 \pm 0.5) \times 10^{-7}$	0.649 ± 0.005	5.3^a

^a Extrapolation of trend of decreasing value with temperature.

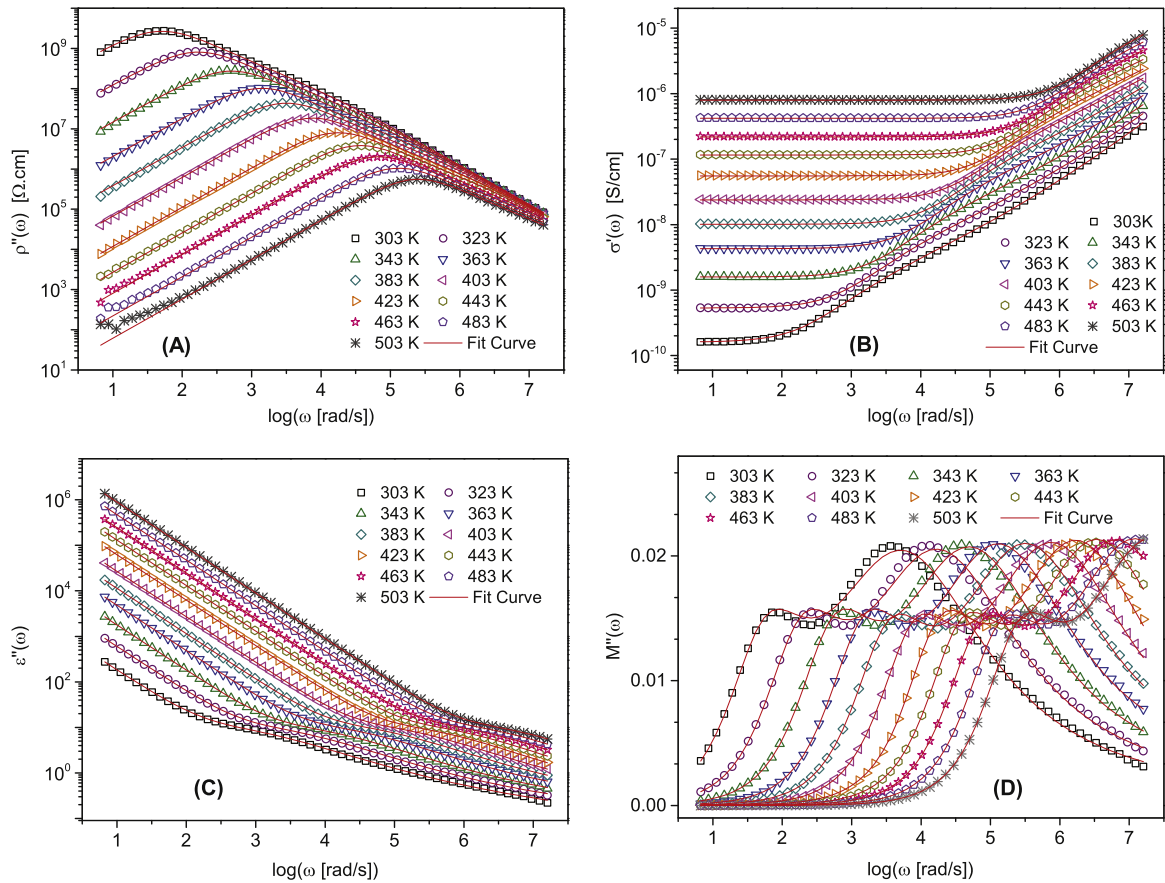


Fig. 4. Complex impedance data of MZFO in different representations (A) $\rho''(\omega)$, (B) $\sigma'(\omega)$, (C) $\epsilon''(\omega)$ and (D) $M''(\omega)$ with fit curve for various temperatures.

The anomalous relaxation due to the distribution of relaxation time can be incorporated by an electrical circuit element such as constant phase element (CPE) [29,28]. Complex impedance of CPE is given by

$$Z_{CPE} = \frac{1}{U(i\omega)^n} \quad (1)$$

where $n\pi/2$ is the constant phase difference between the applied voltage and the current. The parameter n has the value $0 \leq n \leq 1$. With parameter $n=1$, CPE acts as an ideal capacitor of capacitance U with $\pi/2$ phase and with parameter $n=0$, CPE acts as ideal resistor of resistance $R=1/U$ with zero phase. As the value of 'n' decreases, CPE deviates from the capacitor and approaches resistance.

The complex admittance of equivalent circuit in Fig. 3 is obtained as

$$Y_{tot}^*(\omega) = Y_c^*(\omega) + Y_d^*(\omega) = \frac{1}{R_c} + U_c(i\omega)^a + \frac{1}{(C_d i\omega)^{-1} + (U_d(i\omega)^b)^{-1}} + iC_\infty\omega = \frac{1 + R_c U_c (i\omega)^a}{R_c} + \frac{iC_d \omega}{1 + C_d V_d (i\omega)^{(1-b)}} + iC_\infty\omega \quad (2)$$

Resistance R_c with CPE_c of parameters U_c and exponent $0 < a \leq 1$ makes Cole–Cole type conduction relaxation, where $a=1$ is the Debye relaxation. Capacitance C_d with CPE_d of parameters U_d and exponent $0 \leq b < 1$ leads to Cole–Cole type dielectric relaxation. When the exponent $b=0$, CPE_d becomes an ideal resistor of

resistance $V_d = 1/U_d$, which is equivalent circuit of Debye dielectric relaxation. Capacitance C_∞ is the electrical equivalent circuit element for high-frequency permittivity limit ϵ_∞ . Combined Debye like ‘pinned dipole’ and ‘free dipole’ relaxation occurs with parameters, $a=1$ and $b=0$.

Complex permittivity can be obtained from $\epsilon^*(\omega) = Y^*(\omega)/iC_0\omega$. Eq. (5) can be realised by considering $\alpha_c = a$, $\alpha_d = (1 - b)$, relaxation time $\tau_c = (R_c U_c)^{1/\alpha_c}$, $\tau_d = (C_d V_d)^{1/\alpha_d}$. The energy dissipation for the combined ‘pinned dipole’ and ‘free dipole’ relaxation can be easily realised with electrical equivalent circuit. The materials possessing electric and dielectric relaxation have current density j_c from ‘pinned dipole’ and j_d from ‘free dipole’ with total current density

$$j_{tot}(t) = j_c(t) + j_d(t). \quad (3)$$

Total complex ac current density $J_{tot}^*(\omega, t)$ for sinusoidal applied field $E(\omega, t)$ can be represented as

$$J_{tot}^*(\omega, t) = i\omega\epsilon_0\epsilon_{tot}^*E(\omega, t) = \sigma_{tot}^*(\omega)E(\omega, t) \quad (4)$$

where $J_{tot}^*(\omega, t) = J_{tot}^*(\omega, t) + iJ_{tot}^*(\omega, t)$. $J_{tot}^*(\omega, t)$ is the current density component in phase with $E(\omega, t)$ and $J_{tot}^*(\omega, t)$ is the current density component $\pi/2$ out of phase with $E(\omega, t)$. In the presence of anomalous relaxation, combined conduction and dielectric process with Cole–Cole type distribution of relaxation time is considered and complex permittivity obtained as:

$$\epsilon_{tot}^*(\omega) = \frac{\sigma_c(1 + (i\omega\tau_c)^{\alpha_c})}{i\epsilon_0\omega} + \frac{\epsilon_d}{1 + (i\omega\tau_d)^{\alpha_d}} + \epsilon_\infty \quad (5)$$

where $\epsilon_{tot}^*(\omega) = \epsilon'_{tot}(\omega) - i\epsilon''_{tot}(\omega)$. Cole–Cole exponent of conduction relaxation α_c has value $0 < \alpha_c \leq 1$ and Cole–Cole exponent of dielectric relaxation α_d has value $0 < \alpha_d \leq 1$. Combined Debye like conduction relaxation and dielectric relaxation is obtained with $\alpha_c=1$ and $\alpha_d=1$. Now the total complex permittivity is

$$\epsilon_{tot}^*(\omega) = \epsilon_c^*(\omega) + \epsilon_d^*(\omega) \quad (6)$$

where $\epsilon_c^*(\omega)$ is the complex permittivity of ‘pinned dipole’ and $\epsilon_d^*(\omega)$ from ‘free dipole’.

The relation between complex conductivity and complex permittivity, $\sigma_{tot}^*(\omega) = i\omega\epsilon_0\epsilon_{tot}^*(\omega)$ leads to the complex conductivity of the combined ‘pinned dipole’ and ‘free dipole’ relaxation as

$$\sigma_{tot}^*(\omega) = \sigma_c + \sigma_c(i\omega\tau_c)^{\alpha_c} + i\omega\epsilon_0\left(\frac{\epsilon_d}{1 + (i\omega\tau_d)^{\alpha_d}} + \epsilon_\infty\right) \quad (7)$$

where $\sigma_{tot}^*(\omega) = \sigma'_{tot}(\omega) + i\sigma''_{tot}(\omega)$. Total complex conductivity is

$$\sigma_{tot}^*(\omega) = \sigma_c^*(\omega) + \sigma_d^*(\omega) = \sigma_c^*(\omega) + i\omega\epsilon_0\epsilon_d^*(\omega) \quad (8)$$

where $\sigma_c^*(\omega)$ is the complex conductivity of ‘pinned dipole’ and $\sigma_d^*(\omega)$ is the complex conductivity from ‘free dipoles’. Hence the

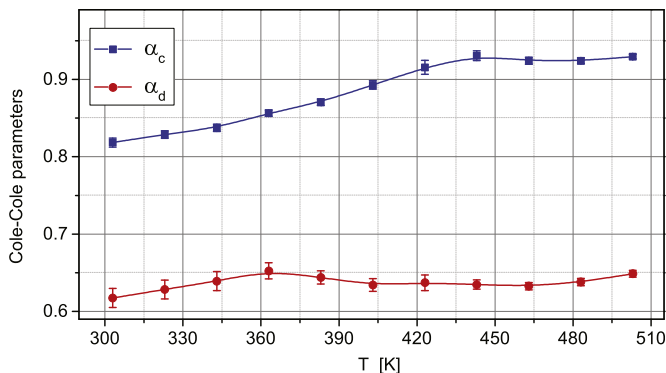


Fig. 5. Temperature dependence of Cole–Cole dielectric relaxation parameter α_d and conductivity relaxation parameter α_c .

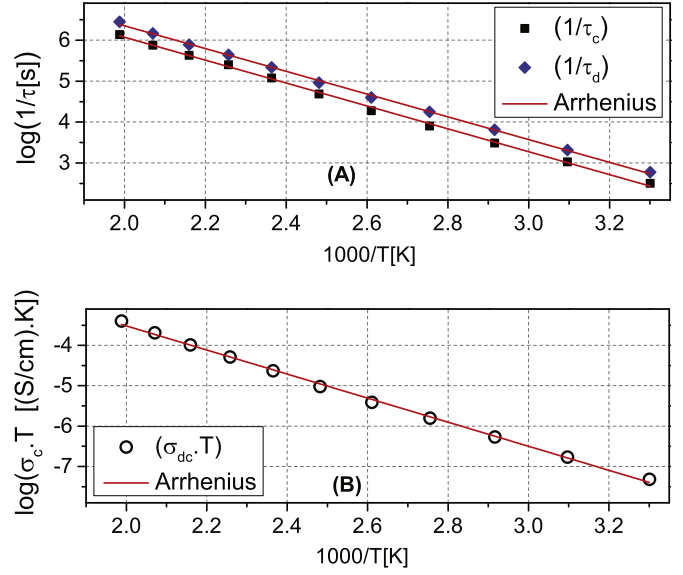


Fig. 6. (A) Arrhenius behaviour of dielectric relaxation time τ_d and conduction relaxation time τ_c . (B) Arrhenius behaviour of conduction.

total complex ac current density $J_{tot}^*(\omega, t)$ becomes

$$J_{tot}^*(\omega, t) = \sigma_c^*(\omega)E(\omega, t) + \epsilon_0\epsilon_d^*(\omega)\frac{\partial E(\omega, t)}{\partial t} \quad (9)$$

where $\sigma_c^*(\omega)$ is the complex conductivity of ‘pinned dipole’ and $\epsilon_d^*(\omega)$ is the complex permittivity of ‘free dipoles’. Fig. 3 shows the schematic representation of ‘pinned dipole’ and ‘free dipole’. The ‘Free dipoles’ try to align in the direction of the applied field with respect to mean position of dipole and produces a reduced field effect in the material. The discontinuous jump of free charge carriers from site to site cause a slower transfer of charge and create a time dependent polarisation during transition. Hence the ‘pinned dipole’ is formed by the hopping free charge and ion lattice. The change of orientation of ‘free dipoles’ does not change the distribution of space charge but the change of orientation of ‘pinned dipoles’ does [30]. It is clear from the literature that the electrical property of the materials can be clearly understood with $\sigma'(\omega)$ and $\epsilon'(\omega)$ data, which are the cause of electric transport and field variation in the material [31]. $\sigma'_{tot}(\omega)$ and $\epsilon'_{tot}(\omega)$ are related with $J_{tot}^*(\omega, t)$ by:

$$J_{tot}^*(\omega, t) = \sigma'_{tot}(\omega)E(\omega, t) + \epsilon_0\epsilon'_{tot}(\omega)\frac{\partial E(\omega, t)}{\partial t} = \sigma'_{tot}(\omega)E(\omega, t) + i\omega\epsilon_0\epsilon'_{tot}(\omega)E(\omega, t) \quad (10)$$

where $\sigma'_{tot}(\omega) = \sigma_c^*(\omega) + \omega\epsilon_0\epsilon_d^*(\omega)$ and $\epsilon'_{tot}(\omega) = \epsilon_d^*(\omega) + \epsilon_\infty(\omega) + \sigma_c^*(\omega)/(\omega\epsilon_0)$ which are individually contributed from the ‘pinned dipole’ and ‘free dipole’. The individual contribution of ‘pinned dipole’ and ‘free dipole’ contribution on current and field can be studied with $\sigma'_{tot}(\omega)$ and $\epsilon'_{tot}(\omega)$:

$$\sigma'_{tot}(\omega) = \sigma_c + \sigma_c\tau_c^{\alpha_c}\omega^{\alpha_c}\cos(\alpha_c\pi/2) + \omega\epsilon_0\epsilon_d^*(\omega) \quad (11)$$

$$\epsilon'_{tot}(\omega) = \frac{\sigma_c\tau_c^{\alpha_c}\omega^{\alpha_c}\sin(\alpha_c\pi/2)}{\omega\epsilon_0} + \epsilon_\infty + \epsilon_d^*(\omega) \quad (12)$$

Complex resistivity of the combined ‘pinned dipole’ and ‘free dipole’ is obtained as $\rho_{tot}^*(\omega) = 1/\sigma_{tot}^*(\omega)$

$$\rho_{tot}^*(\omega) = \frac{1}{\sigma_c(1 + (i\omega\tau_c)^{\alpha_c}) + i\epsilon_0\omega\left(\epsilon_\infty + \frac{\epsilon_d}{1 + (i\omega\tau_d)^{\alpha_d}}\right)} \quad (13)$$

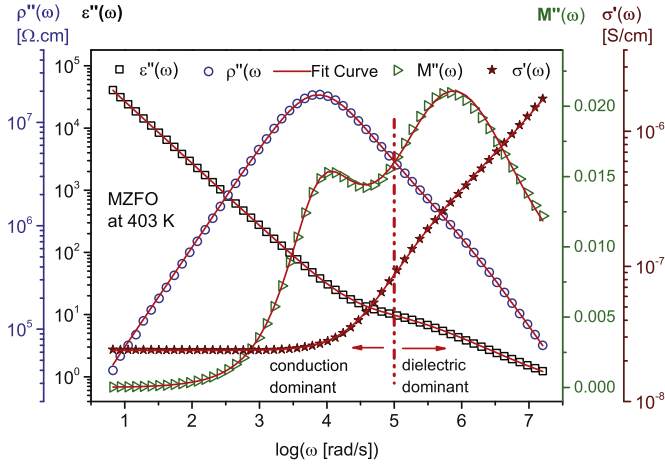


Fig. 7. Conduction relaxation and dielectric relaxation effect on $\rho''(\omega)$, $\epsilon''(\omega)$, $M''(\omega)$ and $\sigma'(\omega)$ of MZFO at temperature 403 K with fit curve. Red dotted line (colour online) shows the boundary of conduction dominant and dielectric relaxation dominant region. (For interpretation of the references to color in this figure caption, the reader is referred to the web version of this paper.)

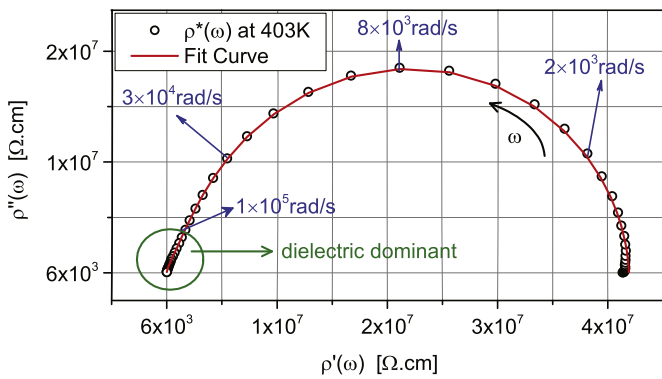


Fig. 8. Nyquist plot of $\rho''(\omega)$ versus $\rho'(\omega)$ of MZFO at 403 K with fit curve.

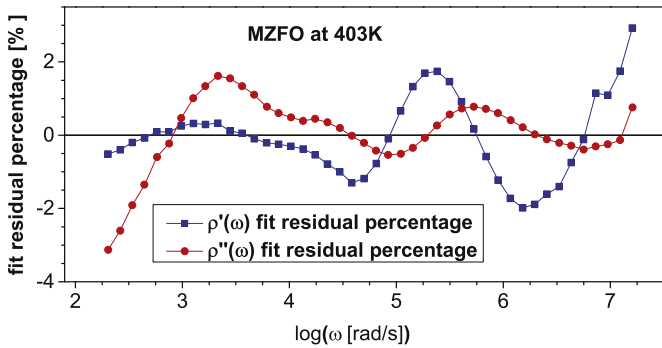


Fig. 9. Fit residual percentage of $\rho'(\omega)$ and $\rho''(\omega)$ of MZFO at temperature 403 K for the combined Cole–Cole type ‘pinned dipole’ and ‘free dipole’ relaxation model.

This is the effective resistivity of the Cole–Cole type dielectric and conductivity relaxation in parallel combination

$$\rho_{tot}^*(\omega) = \rho_c^*(\omega) \parallel \rho_d^*(\omega) \quad (14)$$

where $\rho_c^*(\omega)$ is the complex resistivity of ‘pinned dipole’ and $\rho_d^*(\omega)$ is from ‘free dipole’. One should note that $\rho_{tot}^*(\omega) \neq \rho_c^*(\omega) + \rho_d^*(\omega)$. Complex electric modulus is defined as $M^*(\omega) = 1/\epsilon^*(\omega)$ and effective complex electric modulus of ‘pinned dipole’ and ‘free dipole’ is obtained as

$$M_{tot}^*(\omega) = i\omega\epsilon_0\rho_{tot}^*(\omega) \quad (15)$$

The dispersive behaviour of ‘pinned dipole’ (first two terms in Eqs. (11) and (12)) is similar to the dispersive behaviour of Sidebottom’s anomalous diffusion model [32] and qualitatively similar to the dispersive behaviour Dyre’s random barrier model [12]. Funke’s MIGRATION model considered the similar dispersive behaviour as the consequence of correlated forward back ward jump of charge carriers [33,34]. Sidebottom observed the two power-law dispersion contributions to $\sigma'(\omega)$ of glasses and suggested that they are originating from different mechanism. Type-I dispersive process is considered for the motion of free charges and type-II dispersive process is associated with the counter charge in the host matrix [25,26]. The present model considered that the dispersion is due to atomic scale inhomogeneity of the system in terms of ‘pinned dipole’ and ‘free dipole’ strengths, related to the conductive and dielectric process. Type-I dispersive process is due to ‘pinned dipoles’ and type-II process due to ‘free dipoles’.

3.2. Relaxation studies of $Mn_{0.5}Zn_{0.5}Fe_2O_4$

Eq. (13) is used in WinFit3.3 (Novocontrol) software for fitting and confirmed again using non-linear complex function fitting of Origin software. The physical parameters which follow simultaneously with data of $\rho'(\omega)$ and $\rho''(\omega)$ are shown in Table 1.

These fit parameters of $\rho^*(\omega)$ are used for other representations namely $\epsilon^*(\omega)$, $\sigma^*(\omega)$ and $M^*(\omega)$. Ac electrical data of MZFO in $\rho'(\omega)$, $\sigma'(\omega)$, $\epsilon''(\omega)$ and $M''(\omega)$ with fit curve for various temperature are shown in Fig. 4(A)–(D).

All the four representations show a good agreement with the electrical parameters obtained in Table 1. The ‘pinned dipole’ relaxation is affected by ‘free dipole’ relaxation at high frequencies. $\rho''(\omega)$ shows a deviation from Cole–Cole electric relation at high frequencies. Conductivity $\sigma'(\omega)$ deviates from the power-law behaviour after the crossover frequency, due to ‘free dipole’ relaxation. Dielectric loss $\epsilon''(\omega)$ shows a relaxation peak which is dominated by the dc conduction contribution. Electric modulus $M''(\omega)$ clearly shows two relaxation processes. Here the two relaxation processes are of different origins. The two different relaxations are attributed to ‘pinned dipole’ relaxation related to conduction process and comparatively fast ‘free dipole’ relaxation related to dielectric process.

The dielectric strength of ‘free dipole’ ϵ_d slightly increases with an increase of temperature, while the limiting high frequency dielectric constant ϵ_∞ decreases with an increase of temperature. Inverse temperature dependence of ϵ_∞ is observed in many systems [35]. It is observed that the value of ϵ_∞ decreases with an increase of temperature, but the exact information on ϵ_∞ are out the frequency window for a few high temperature data. The trend of decrease of ϵ_∞ has been followed for data analysis of such temperatures. The Cole–Cole parameter ‘ α_d ’ is the measure of the symmetrical broadening of dielectric loss peak. Cole–Cole behaviour occurs due to the many body effect of interacting dipoles. Understanding the physical mechanism underlying Cole–Cole behaviour is challenging [36]. The ‘free dipole’ relaxation exponent ‘ α_d ’ of MZFO is weakly temperature dependent and it is shown in Fig. 5.

It shows that the relaxation time of free dipoles is distributed symmetrically with respect to τ_d and the distribution is weakly temperature dependent. The dielectric relaxation time τ_d for various temperatures is shown in Fig. 6(A). ‘Free dipole’ relaxation is thermally activated process and follows Arrhenius behaviour,

$$\frac{1}{\tau_d(T)} = \frac{1}{\tau_{T\infty}} \exp[-E_d/k_B T] \quad (16)$$

where k_B is the Boltzmann constant, T is the absolute temperature and $\tau_{T\infty}$ is the relaxation time at infinite temperature. ‘Free dipole’

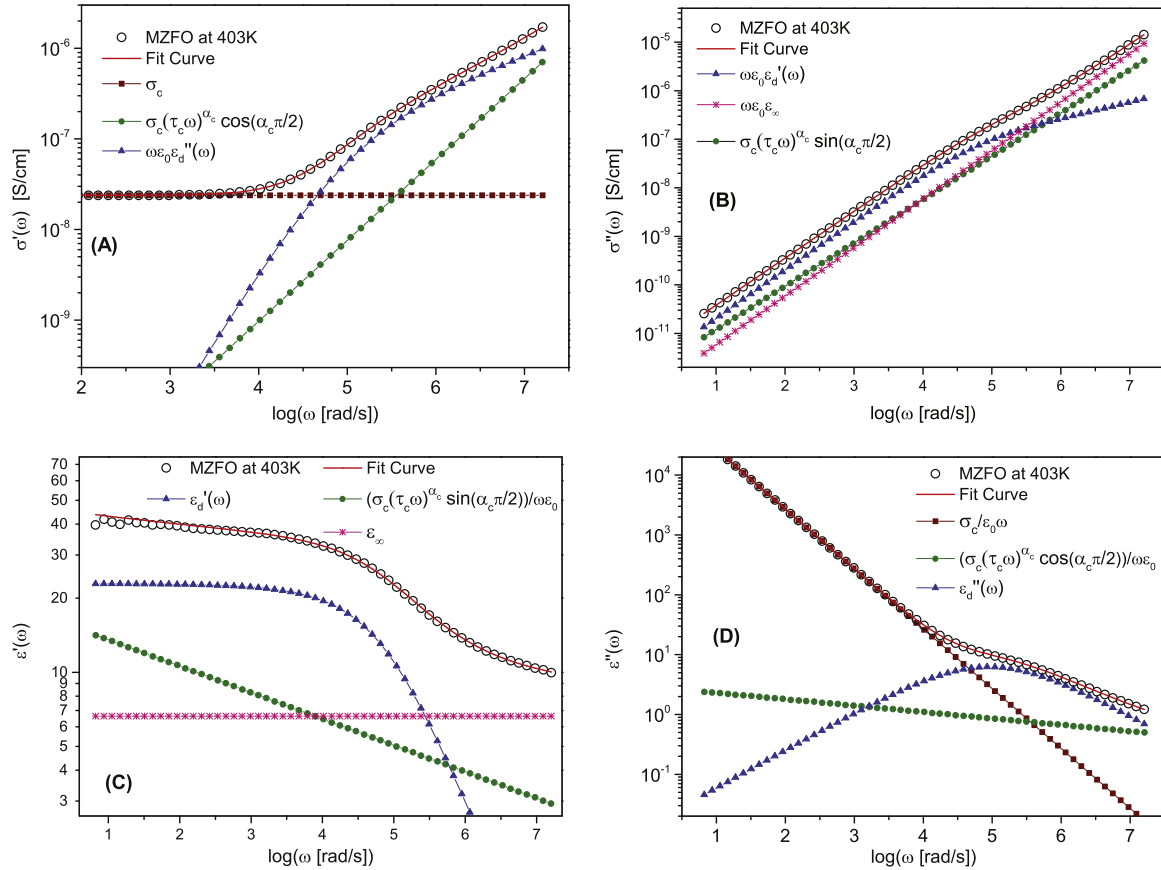


Fig. 10. (A)–(D) show, individual conduction and dielectric relaxation contribution to $\sigma'(\omega)$, $\sigma''(\omega)$, $\epsilon'(\omega)$ and $\epsilon''(\omega)$ of dielectric and conduction relaxation to of MZFO at temperature 403 K respectively, as a function of frequency.

activation energy of MZFO is 0.55 ± 0.02 eV and τ_{∞} of MZFO is $(7.9 \pm 1.2) \times 10^{11} \text{ s}^{-1}$.

The dc conductivity of the material decreases systematically with an increase of temperature which is expected for semi-conducting type materials which is shown in Fig. 6(B). Conductivity follows Arrhenius type hopping conduction,

$$\sigma_c(T) = \frac{A}{T} \exp[-E_\sigma/k_B T] \quad (17)$$

where A is the pre-exponential factor and E_σ is the activation energy for conduction. Activation energy E_σ obtained for MZFO is 0.59 ± 0.02 eV. Hopping charges and hence the 'pinned dipole' relaxation are thermally activated process which follow Arrhenius relation,

$$\frac{1}{\tau_c(T)} = \frac{1}{\tau_0} \exp[-E_h/k_B T] \quad (18)$$

where $1/\tau_0$ is the attempt jump for charge carriers in the material with activation energy E_h . The number of successful jumps $1/\tau_c(T)$ is a function of temperature which is governed by attempt jump $1/\tau_0$ and activation energy of hopping E_h . Charge carriers of MZFO have attempt jump $(4.5 \pm 1.0) \times 10^{11} \text{ s}^{-1}$ and activation energy of hopping is 0.55 ± 0.02 eV. Due to the hopping of charge carriers, its neighbouring sites may create a mismatch and hence backward jump to its original site is possible. This may leads to a correlated forward backward hopping of charge carriers [33]. Ac conductivity power-law is a consequence of reiterative hopping. Ac conductivity and dc conductivity are directly related to each other and ac conductivity exhibits a lower activation energy [25]. The non-Debye parameter α_c of conduction relaxation slightly increases

with an increase of temperature as shown in Fig. 5. It shows that the relaxation time of 'pinned dipoles' is distributed symmetrically with respect to τ_c and the distribution varies with temperature. Combined effect of disorder and Coulomb interaction provides non-Debye relaxation [37,38]. Increase of temperature reduces the Coulombic interaction of pinned dipoles approaching to Debye type relaxation. The 'free dipole' relaxation occurs at higher frequencies compared with 'pinned dipole' relaxation and hence the relaxation current density at shorter time scales will be dominated by 'free dipole' and at longer time scale by 'pinned dipole'.

Ac electrical data of MZFO in $\epsilon'(\omega)$, $\rho'(\omega)$, $M''(\omega)$ and $\sigma''(\omega)$ at temperature 403 K is shown in Fig. 7. Fit curve of combined 'pinned dipole' and 'free dipole' relaxation shows good agreement in all the representations. Red dotted line (colour online) separates the pinned dipole relaxation (conduction) dominant and free dipole relaxation (dielectric relaxation) dominant region in each representation. Nyquist plot of $\rho'(\omega)$ versus $\rho''(\omega)$ is shown in Fig. 8 with fit curve. The fit residues of 'pinned dipole' and 'free dipole' relaxation are always less than 3% and it is shown in Fig. 9.

Individual contribution of 'pinned dipole' and 'free dipole' on $\sigma'_{tot}(\omega)$, $\sigma''_{tot}(\omega)$, $\epsilon'_{tot}(\omega)$ and $\epsilon''_{tot}(\omega)$ at temperature 403 K is shown in Fig. 10(A)–(D). Fig. 10(A) clearly shows that $\sigma'_{tot}(\omega)$ has two different dispersive processes. $\sigma'_{tot}(\omega)$ of the material is contributed by the dc conductivity σ_c and ac conductivity $\sigma_{ac} = \sigma_c \tau_c^{\alpha_c} \omega^{\alpha_c} \cos(\alpha_c \pi/2)$, which is in the form of power-law with an additional factor of $\cos(\alpha_c \pi/2)$. In addition to this, the imaginary part of dielectric relaxation contributes $\omega \epsilon_0 \epsilon_d''(\omega)$, which makes deviation from power law behaviour of $\sigma'(\omega)$ at high frequencies. Dielectric constant $\epsilon'_{tot}(\omega)$ of the material is contributed by the real part of the dielectric relaxation $\epsilon_d'(\omega)$ due to the 'free dipole' and frequency independent high frequency permittivity ϵ_∞ . 'Pinned dipole'

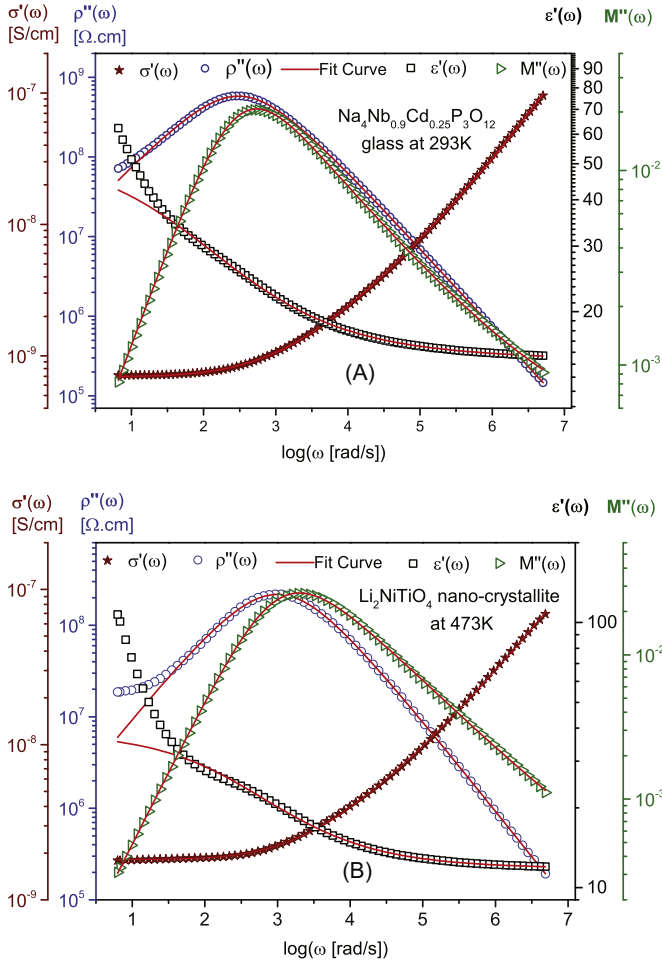


Fig. 11. $\sigma'(\omega)$, $\rho''(\omega)$, $\epsilon'(\omega)$ and $M''(\omega)$ with combined 'pinned dipole' and 'free dipole' relaxation fit of (A) $\text{Na}_4\text{Nb}_{0.9}\text{Cd}_{0.25}\text{P}_3\text{O}_{12}$ glass at temperature 293 K and (B) mixed electronic–ionic conducting $\text{Li}_2\text{NiZrO}_4$ at 473 K.

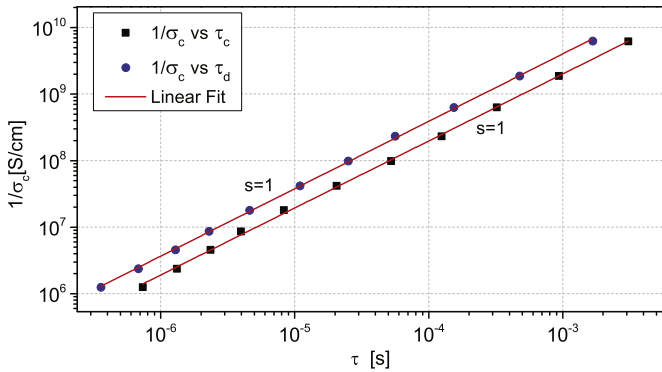


Fig. 12. $1/\sigma_c$ versus conduction relaxation time τ_c and dielectric relaxation time τ_d in log–log scale. The straight line has slope, $s=1$ for both pinned and free dipole relaxation.

relaxation contributes $\sigma_c \tau_c^{\alpha_c} \omega^{\alpha_c} \sin(\alpha_c \pi/2) / \omega \epsilon_0$, to the dielectric constant, which makes the dielectric constant $\epsilon'_{tot}(\omega)$ frequency dependent at low frequencies. $\epsilon'_{tot}(\omega)$ has the relaxation peak from $\epsilon''_d(\omega)$ and dc conductivity contribution and ac conductivity contribution are shown in Fig. 10(D).

The present combined 'free dipole' and 'pinned dipole' relaxation model is applicable for not only semiconducting materials but also ionic conducting solids. Complex impedance data of our

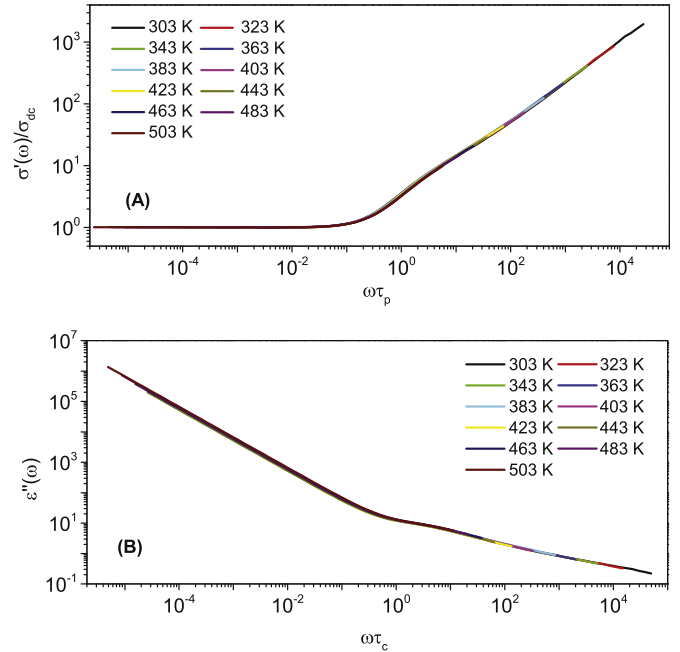


Fig. 13. Time temperature scaling of (A) $\sigma'(\omega)$ with dielectric relaxation time τ_d and (B) $\epsilon''(\omega)$ with conduction relaxation time τ_c .

earlier studies on ionic conducting glass $\text{Na}_4\text{Nb}_{0.9}\text{Cd}_{0.25}\text{P}_3\text{O}_{12}$ [39] and mixed electronic–ionic conducting $\text{Li}_2\text{NiZrO}_4$ [40] show a good agreement with the combined 'pinned dipole' and 'free dipole' relaxation and follows all representations. Ac electrical data of $\text{Na}_4\text{Nb}_{0.9}\text{Cd}_{0.25}\text{P}_3\text{O}_{12}$ at temperature 293 K and $\text{Li}_2\text{NiZrO}_4$ at 473 K with fit curve are shown in Fig. 11(A) and (B). The low frequency electrode polarisation or Maxwell–Wagner polarisation is not considered in the present model. Detailed analysis of ac electrical data of various systems for the present model may be in our future works.

Time–temperature superposition can be utilised as a tool to determine the invariance of physical mechanism of the process with thermodynamic parameters such as pressure and temperature [41–43]. Dc conductivity σ_c and relaxation time τ_c are correlated with Barton–Nakajima–Namikawa relation [24]. Time–temperature scaling of $\sigma'(\omega, T)$ with conduction relaxation time τ_c indicates the correlation of conduction with the relaxation [24,41,42]. In the dielectric relaxation dominant systems, the dielectric relaxation of structural process is coupled with dc conduction by DSE relation, $\sigma_c \tau_d = \text{constant}$ or decoupled with fractional power of τ_d known as fractional DSE equation [4]. In the present study, it is observed that the 'pinned dipole' relaxation τ_c and 'free dipole' relaxation τ_d of MZFO are of the same activation energy. Both τ_c and τ_d are proportional to $1/\sigma_c$ with slope, $s=1$ and it is shown in Fig. 12. This indicates that τ_c , τ_d are coupled with $\sigma'(\omega, T)$ and it can be scaled with either τ_c or τ_d . Scaling of $\sigma'(\omega)$ with τ_d and $\epsilon''(\omega, T)$ with τ_c is shown in Fig. 13.

The two relaxation processes in MZFO are modelled with two Cole–Cole conduction processes, in our earlier work [44]. The activation energies of conduction ($0.59 \text{ eV} \pm 0.02 \text{ eV}$) and hopping ($0.55 \text{ eV} \pm 0.02 \text{ eV}$) of the 'pinned dipole' of the present model are the same as the activation energy of conduction ($0.59 \text{ eV} \pm 0.02 \text{ eV}$) and hopping ($0.54 \text{ eV} \pm 0.02 \text{ eV}$) of one of the processes of 'two Cole–Cole conduction' method. The physical process of 'free dipole' in the present model and the second process (second layer) of 'two Cole–Cole conduction' model are entirely different. In the present model the system is considered as inhomogeneous to atomic scale which generates 'pinned dipoles'

and 'free dipoles', while 'two layer conduction model' considered the system with macroscopic inhomogeneity of two layers of different capacitances and resistances. The second layer of 'two Cole–Cole conduction' model has the electrical conduction with activation energy $0.59 \text{ eV} \pm 0.02 \text{ eV}$ and hopping with activation energy $0.43 \text{ eV} \pm 0.02 \text{ eV}$ [44]. On the other hand, 'free dipoles' of the present model are coupled with hopping process with activation energy $0.55 \text{ eV} \pm 0.02 \text{ eV}$. In the present experimental data the strong Maxwell type apparent relaxation is absent [45–47]. The measurement on the present sample has been carried out during heating and cooling in nitrogen atmosphere. During heating cycle the present sample shows Maxwell type 'apparent' relaxations with orders of magnitude 10^4 at low frequencies, at low temperatures. This 'apparent' relaxation disappears with an increase of temperature and does not show with measurements during cooling [48]. The absorbed water in materials may cause a large value of $\epsilon''(\omega)$ at room temperature but it may disappear by heating [49]. Various preparation methods of Mn–Zn ferrite show dielectric loss peak and absence of Maxwell–Wagner type apparent relaxation [50,51] as in the present data. There are reports on nano scale MZFO with very low Maxwell–Wagner apparent relaxation [52], while MZFO prepared with ceramic route has very large Maxwell–Wagner apparent relaxation [53]. The details on the presence or absence of strong Maxwell–Wagner apparent relaxation require a more systematic study on given material and different materials based on various microstructures and measurements in various conditions.

Time temperature superposition indicates that the physical mechanism of 'pinned dipole' and 'free dipole' relaxations of MZFO is independent of temperature and dc conduction is coupled with both the relaxation processes. The microscopic understanding of 'pinned dipole' and 'free dipole' in MZFO may be realised as follows. XRD and Raman spectra of the sample confirm the spinel structured $\text{Mn}_{0.5}\text{Zn}_{0.5}\text{Fe}_2\text{O}_4$ with disorder. Unit cell of MZFO with 32 oxygen atoms form 64 tetrahedral (A-Sites) and 32 octahedral (B-sites). Eight of the A-sites preferably with 2^+ cation and 16 B-sites preferably with 3^+ cation form the spinel structure. It is not necessary that the 2^+ ions must reside on B-site and 3^+ cation must reside on A-site for nano-phase materials. 2^+ ions and 3^+ ions may be distributed between both kinds of site [22,54]. Distribution of cation may displace away the oxygen atoms from A-site cation, relative to ideal face centred cubic lattice. In MZFO, Mn has more tetrahedral affinity than Fe cation [22]. The mean distance between the cation and the oxygen may differ from cation excited of 2^+ and 3^+ states in the same kind of site. This disorder is larger for manganese in comparison with iron than zinc [22]. These effects on cation anion distribution may create the 'free dipole' effect and hence the dielectric relaxation. The electrical conductivity of MZFO depends on the cation distribution along with its oxidation states. Both the hole hopping of $\text{Mn}^{2+} - \text{Mn}^{3+}$ and the electron hopping of $\text{Fe}^{3+} - \text{Fe}^{2+}$ can happen to the system [17,18] which may lead to the formation of 'pinned dipoles'.

4. Conclusion

The relaxation concepts of 'semiconductor school' and 'dielectric school' have been combined by considering combined 'pinned dipole' and 'free dipole' relaxations. Different representations of ac electrical data namely $\rho^*(\omega)$, $\epsilon^*(\omega)$, $\sigma^*(\omega)$ and $M^*(\omega)$ are formulated for the combined Cole–Cole type of 'pinned dipole' and 'free dipole' relaxation. Cole–Cole type relaxation of combined 'pinned dipole' and 'free dipole' relaxation is realised with electrical equivalent circuit. The ac electrical data of MZFO show influence of dielectric loss peak at high frequencies and the combined 'pinned dipole' and 'free dipole' relaxation shows excellent

fit with the experimental data. The electrical parameters obtained show a good agreement with all the ac electrical representations. Combined 'pinned dipole' and 'free dipole' has very good fit residue. Ac conductivity has two dispersive contributions, from the pinned dipole associated with conduction process and free dipole associated with the dielectric process. Individual current contributions of 'pinned dipoles' and 'free dipoles' are obtained from the experimental ac electrical data. For MZFO, the 'pinned dipoles' and 'free dipoles' have the same activation energy, and τ_c and τ_d are correlated with dc conductivity σ_c . The 'pinned dipole' relaxation τ_c and 'free dipole' relaxation τ_d show that the processes are coupled and follows time–temperature scaling in both τ_c and τ_d . Possible origin of 'pinned dipole' and 'free dipole' of MZFO is discussed. Combined 'pinned dipole' and 'free dipole' relaxation gives better and unique insight to the relaxation process regardless the way of representation.

Acknowledgements

Authors thank Central Instrumentation Facility, Pondicherry University for the dielectric spectroscopy measurements and CSIR project 03(1279)/13/EMR-II for financial support. One of the authors (N.S.K.K.) acknowledges DST-PURSE SR/S9/Z-23/2010/36 for the financial support as project assistant.

Appendix A. Supplementary data

Supplementary data associated with this paper can be found in the online version at <http://dx.doi.org/10.1016/j.physb.2016.02.018>.

References

- [1] U. Sailaja, M.S. Thayyil, N.S.K. Kumar, G. Govindaraj, *Eur. J. Pharm. Sci.* 49 (2012) 333.
- [2] M. Shahin, S.S.N. Murthy, *J. Chem. Phys.* 118 (2003) 7495.
- [3] Z. Wojnarowska, K.J. Paluch, L. Tajner, K. Grzybowska, K.L. Ngai, M. Paluch, *Phys. Chem. Chem. Phys.* 15 (2013) 9205.
- [4] S. Corezzi, E. Campani, P.A. Rolla, S. Capaccioli, D. Fioretto, *J. Chem. Phys.* 111 (1999) 9343.
- [5] S.V. Rathan, G. Govindaraj, *Mater. Chem. Phys.* 120 (2010) 255.
- [6] S.V. Rathan, G. Govindaraj, *Solid State Sci.* 12 (2010) 730.
- [7] R. Cheruku, G. Govindaraj, L. Vijayan, *Mater. Chem. Phys.* 141 (2013) 620.
- [8] L. Vijayan, R. Cheruku, G. Govindaraj, *J. Appl. Phys.* 111 (2012) 064905.
- [9] L. Vijayan, G. Govindaraj, *J. Phys. Chem. Solids* 72 (2011) 613.
- [10] N.S.K. Kumar, T.S. Shahid, G. Govindaraj, *Int. J. ChemTech Res.* 6 (2014) 2213.
- [11] N. Sivakumar, A. Narayanasamy, N. Ponpandian, G. Govindaraj, *J. Appl. Phys.* 101 (2007) 084116.
- [12] J.C. Dyre, *J. Appl. Phys.* 64 (1988) 2456.
- [13] K.L. Ngai, R.W. Rendell, *Phys. Rev. B* 61 (2000) 9393.
- [14] D.L. Sidebottom, B. Roling, K. Funke, *Phys. Rev. B* 63 (2000) 024301.
- [15] I.M. Hodge, K.L. Ngai, C.T. Moynihan, *J. Non-Cryst. Solids* 351 (2005) 104.
- [16] J.C. Dyre, *Phys. Rev. Lett.* 110 (2013) 245901.
- [17] E.V. Goopalan, K.A. Malini, D.S. Kumar, Y. Yoshida, I.A. Al-Omari, S. Saravanan, M.R. Anantharaman, *J. Phys.: Condens. Matter* 21 (2009) 146006.
- [18] E.V. Goopalan, K.A. Malini, S. Sagar, D.S. Kumar, Y. Yoshida, I.A. Al-Omari, S. Saravanan, M.R. Anantharaman, *J. Phys. D: Appl. Phys.* 42 (2009) 165005.
- [19] M. Younas, M. Nadeem, M. Atif, R. Grossinger, *J. Appl. Phys.* 109 (2011) 093704.
- [20] A. Arunkumar, D. Vanidha, K. Oudayakumar, S. Rajagopan, R. Kannan, *J. Appl. Phys.* 114 (2013) 183905.
- [21] D. Varshney, K. Verma, A. Kumar, *Mater. Chem. Phys.* 131 (2011) 413.
- [22] S. Calvin, E.E. Carpenter, B. Ravel, V.G. Harris, S.A. Morrison, *Phys. Rev. B* 66 (2002) 224405.
- [23] C. Rath, S. Anand, R.P. Das, K.K. Sahu, S.D. Kulkarni, S.K. Date, N.C. Mishra, *J. Appl. Phys.* 91 (2002) 2211.
- [24] J.C. Dyre, T.B. Schroder, *Rev. Mod. Phys.* 72 (2000) 873.
- [25] D.L. Sidebottom, P.F. Green, R.K. Brow, *Phys. Rev. Lett.* 74 (1995) 5068.
- [26] S.R. Elliot, *Solid State Ionics* 27 (1994) 70.
- [27] F. Kremer, A. Schonhals (Eds.), *Broad Band Dielectric Spectroscopy*, 1st ed., Springer, Berlin, 2002.
- [28] E. Barsoukov, J.R. Macdonald (Eds.), *Impedance Spectroscopy Theory, Experiment and Applications*, 2nd ed., John Wiley and Sons, New Jersey, 2005.
- [29] B.A. Boukamp, *Solid State Ionics* 18–19 (1986) 136.

- [30] A.K. Jonscher, *Nature* 253 (1975) 717.
- [31] D.L. Sidebottom, *Rev. Mod. Phys.* 81 (2009) 999.
- [32] D.L. Sidebottom, P.F. Green, R.K. Brow, *Phys. Rev. B* 51 (1995) 2770.
- [33] K. Funke, R.D. Banhatti, S. Bruckner, C. Cramer, C. Krieger, A. Mandanici, C. Martini, I. Ross, *Phys. Chem. Chem. Phys.* 4 (2002) 3155.
- [34] N.S.K. Kumar, S.V. Rathan, G. Govindaraj, *IOP Conf. Ser.: Mater. Sci. Eng.* 73 (2015) 012066.
- [35] K.L. Ngai, *Relaxation and Diffusion in Complex Systems*, Springer, London, 2011.
- [36] A. Puzenko, P.B. Ishai, Y. Feldman, *Phys. Rev. Lett.* 105 (2010) 037601.
- [37] P. Maass, J. Petersen, A. Bunde, W. Dieterich, H.E. Roman, *Phys. Rev. Lett.* 66 (1991) 52.
- [38] B. Roling, C. Martiny, S. Bruckner, *Phys. Rev. B* 63 (2001) 214203.
- [39] N.S.K. Kumar, G. Govindaraj, *AIP Conf. Proc.* 1591 (2014) 759.
- [40] R. Cheruku, G. Govindaraj, L. Vijayan, *Mater. Chem. Phys.* 141 (2013) 620.
- [41] D.L. Sidebottom, J. Zhang, *Phys. Rev. B* 62 (2000) 5503.
- [42] A. Ghosh, A. Pan, *Phys. Rev. Lett.* 84 (2000) 2188.
- [43] C.R. Mariappan, G. Govindaraj, *J. Mater. Sci. Lett.* 21 (2002) 1401.
- [44] N.S.K. Kumar, T.S. Shahid, G. Govindaraj, *AIP Conf. Proc.* 1665 (2015) 110041.
- [45] C.G. Koops, *Phys. Rev.* 83 (1951) 111.
- [46] J.C. Maxwell, *Electricity and Magnetism*, vol. 1, Oxford University Press, London, 1873.
- [47] K.W. Wagner, *Ann. Phys.* 40 (1913) 817.
- [48] N.S.K. Kumar, T.S. Shahid, G. Govindaraj, Investigation on conductivity anomalies in ferrites using impedance spectroscopy, *Results Phys.*, In Press, <http://dx.doi.org/10.1016/j.rinp.2015.12.005>.
- [49] K. Iwauchi, *Jap. J. Appl. Phys.* 10 (1971) 1520.
- [50] S. Bhagwat, P. Rao, *IOSR J. Appl. Phys.* 3 (2013) 2278.
- [51] C. Venkataraju, G.S.K. Sivakumar, *J. Magn. Magn. Mater.* 323 (2011) 1817.
- [52] K. Murugesan, P.M.M. Gazzali, B. Sathyamoorthy, G. Chandrasekaran, *AIP Conf. Proc.* 1512 (2013) 314.
- [53] K. Latha, K.S. Mohan, D. Ravinder, *Phys. Status Solidi A* 142 (1994) K103.
- [54] J. Smit, H.P.J. Wijn, *Ferrites*, New York, Wiley, 1959.